ADVANCED OPTICAL MATERIALS
www.advopticalmat.de

Stereoisomeric Homo- and Hetero-Binuclear Iridium(III) Complexes with 3-Oxidopicolinate Bridging Ligand and Their Application in OLEDs

Kochan Sathyaseelan Bejoymohandas, Andrea Baschieri, Francesco Reginato, Stefano Toffanin, Mario Prosa, Elisa Bandini, Andrea Mazzanti, and Filippo Monti**

The small and simple 3-hydroxypyridine-2-carboxylic acid (Hpic-OH) is explored as asymmetric bridging ligand for the synthesis of neutral binuclear cyclometalated iridium(III) complexes. Once fully deprotonated the $picO^{2-}$ ligand can act as ancillary ligand toward two iridium centers adopting both the N^O⁻ and O^O⁻ chelation modes. To tune the energy of the excited states within such binuclear complexes, the 2-(2,4-difluorophenyl)pyridine (Hdfppy) and the 2-phenylbenzothiazole (Hpbtz) are used as cyclometalating ligands to respectively obtain both blue- or orange-emissive homo-cyclometalated complexes (BB and YY, with formula $[Ir(dfppy)_2]_2(picO)$ and $[Ir(pbtz)_2]_2(picO)$, respectively). Moreover, for the first time, short-bridged hetero-cyclometalated binuclear complexes are also obtained (BY and YB, with formula $[Ir(dfppy)_2](picO)[Ir(pbtz)_2]$ and $[Ir(pbtz)_2](picO)[Ir(dfppy)_2]$). Depending on the reciprocal arrangement of the cyclometalating ligands on the two sides of the small picolinate bridge, two couples of diastereoisomers are obtained and efficiently separated, as proved by combined NMR and DFT studies. The reported binuclear complexes are highly emissive with photoluminescence quantum yields (PLQYs) up to 67%, which are comparable to those of their mononuclear analogues (B and Y). Due to the full reversibility of their redox processes, all the complexes are also tested in solution-processed organic light-emitting diodes, providing unique OLEDs based on hetero-binuclear cyclometalated iridium(III) complexes.

1. Introduction

Phosphorescent cyclometalated heteroleptic and homoleptic mononuclear iridium(III) complexes have been extensively studied due to their highly efficient and tuneable emission[1,2] making them suitable as luminescent materials in full-color organic light-emitting devices (OLEDs),[3,4] white-light sources,[5] and biosensors for bio-diagnostic[6,7] and bioimaging.[8,9] Moreover, due to strong spin–orbit coupling (SOC) induced by a heavy transition metal,[10,11] cyclometalated iridium(III) complexes are ideal active materials in OLEDs since they can utilize both the singlet and triplet excitons; in addition, because of their high quantum yields and short excited-state lifetimes, they can even convert more excitons per unit of time into photon output.[12]

The tuning of the emission color in iridium(III) complexes is mainly achieved by chemically modifying the organic ligands (cyclometalated or ancillary) leading to emitting excited states of different nature and energy.[1,13,14] Two main strategies are widely used: i) adjusting the conjugated system of cyclometalated ligands;[15] ii) changing the functional groups on the ligands;[16] such strategies can also be combined to achieve better results.[17,18] Of course, the skeleton of cyclometalated or ancillary ligands can also be modified to tune the emission colors too.[19] However, no matter which one of the above strategies is adopted, the key point always focuses on playing on the organic ligands, always leading to the

K. S. Bejoymohandas, A. Baschieri, E. Bandini, F. Monti
Institute for Organic Synthesis and Photoreactivity (ISOF)
National Research Council of Italy (CNR)
Via Piero Gobetti 101, Bologna I-40129, Italy
E-mail: filippo.monti@isof.cnr.it

The ORCID identification number(s) for the author(s) of this article can be found under https://doi.org/10.1002/adom.202401586

DOI: 10.1002/adom.202401586

F. Reginato, S. Toffanin, M. Prosa
Institute of Nanostructured Materials (ISMN)
National Research Council of Italy (CNR)
Via Piero Gobetti 101, Bologna I-40129, Italy
E-mail: mario.prosa@cnr.it

A. Mazzanti
Department of Industrial Chemistry "Toso Montanari"
University of Bologna
Via Piero Gobetti 85, Bologna I-40129, Italy

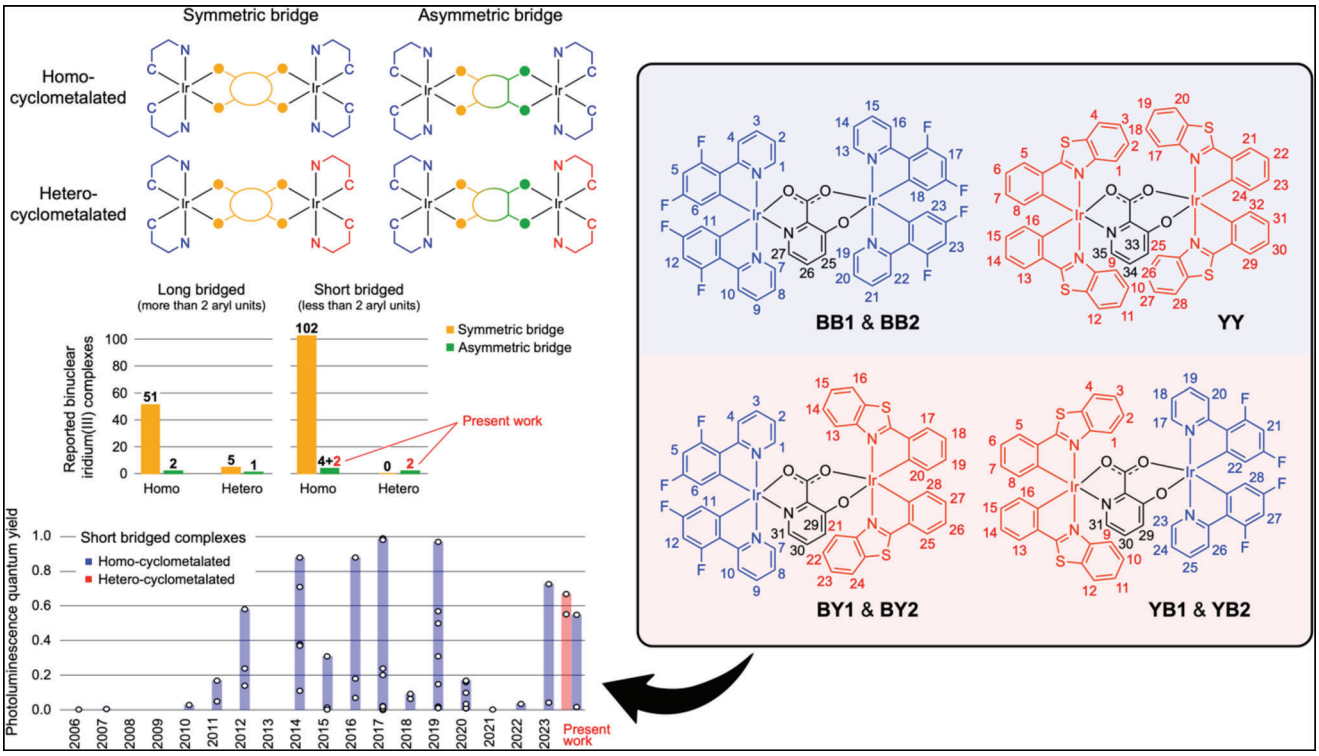

Figure 1. (Left) Summary of bibliographic survey on examples of binuclear iridium(III) complexes reported in the literature, classified based on the symmetry and size of the bridging unit, and on the presence of identical or different cyclometalating ligands on the two iridium centers. Photoluminescence quantum yields are also reported for all the investigated compounds. (Right) Cyclometalated binuclear iridium(III) complexes investigated in the present work.

formation of iridium complexes with just one iridium(III) centre.

In contrast to mononuclear complexes, cyclometalated binuclear counterparts are rarely investigated since more synthetically challenging and usually less emissive,[20,21] so that their applications are under-explored (e.g., they are considered less suitable for OLEDs).[21–28] However, the above-mentioned issues can be overcome by judicious molecular design.[14,28,29–38] Highly flexible bridges should be avoided since they promote non-radiative processes, weakening emission output; indeed, rigid bridging units are usually used to achieve high PLQYs in binuclear iridium complexes.[29,39]

Just like chemically engineering the ligands tunes the emission color of the related complex,[22,40] the incorporation of a second iridium(III) centre into conventional mononuclear complexes provides extra degrees of freedom in boosting the properties of the systems such as: i) exploring new structural chemistry via the bridging ligand;[22,41] ii) increasing the spin-orbit coupling due to the presence of two metal centres, which may further increase the radiative rate constants (k_r);[42,43] iii) easier access to efficient red emitters due to highly conjugated bridging units;[11,32] iv) possible dual emission due to partial energy transfer between uncoupled excited states of different nature.[36] As shown in **Figure 1**, the most explored class of binuclear iridium(III) complexes are based on rigid symmetric bridges (i.e., 158 vs 7 cases reported so far, see Table S1, Supporting Information for individual references).

Moreover, within this class, the vast majority of such complexes are homo-cyclometalated (i.e., both iridium centres have the same cyclometalating ligands), since this is the easiest way to synthesise a binuclear complex; anyway, such approach basically covalently links together two identical mononuclear moieties with identical photophysical properties. A valid approach to diversify such moieties in a binuclear iridium(III) complex with a symmetric bridge is to attach different cyclometalating ligands to the two iridium centres; this route is limited so far to just five examples (see Figure 1; Table S1, Supporting Information).

On the contrary, if an asymmetric bridging ligand is used, both homo- and hetero-cyclometalated complexes result into two different iridium centres with distinct properties. This class of compounds is also rather rare with 6 homo- and only 1 hetero-binuclear cyclometalated complexes reported so far (Figure 1). In the present work, we present other 4 examples of such unexplored class of complexes (i.e., 2 homo- and 2 hetero-cyclometalated compounds). In our investigation, we used the 3-hydroxypyridine-2-carboxylic acid (**Hpic-OH**) as a very simple and small bridge but displaying high structural rigidity. Moreover, once fully deprotonated, such 3-oxidopicolinate ligand (**pic-O^{2-}**) has the ability to coordinate two metal centres through NˆO and OˆO chelation modes, forming neutral binuclear iridium(III) complexes with a short asymmetric bridge (Figure 1).

However, due to the chiral nature of the two octahedral metal centres and the asymmetry of our ancillary ligand, mixtures of *rac*-(ΛΔ'/ΔΛ') and *rac*-(ΔΔ'/ΛΛ') diastereomers were obtained

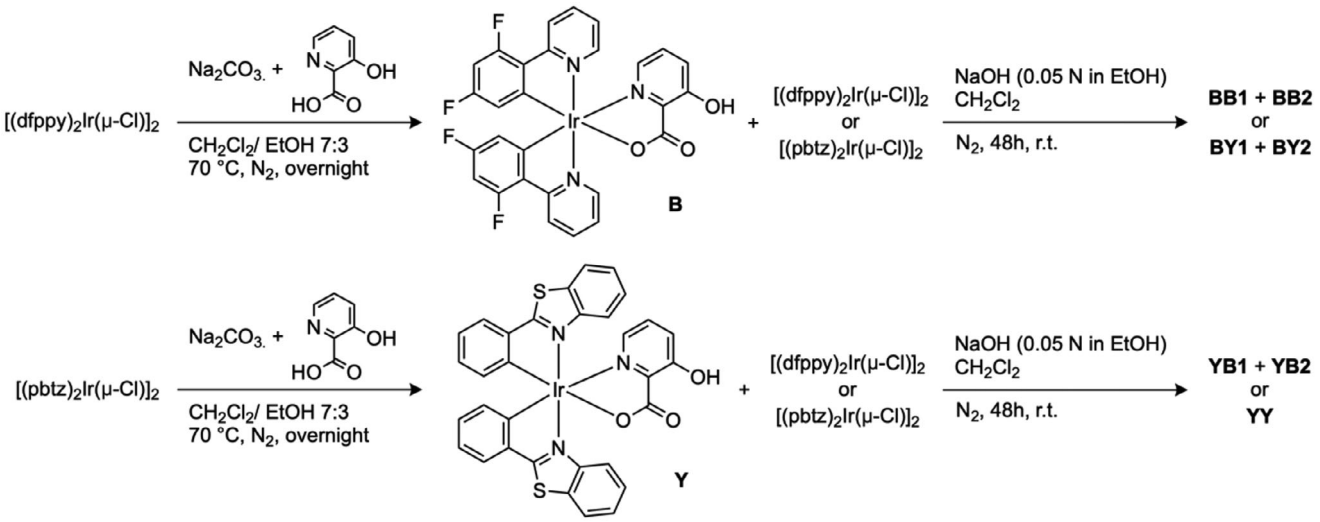

Scheme 1. Synthesis of the mononuclear and binuclear cyclometalated iridium(III) complexes.

for all of the complexes, as commonly observed for binuclear complexes featuring Ir–Ir distances greater than ≈5 Å.[41] Notably, due to our asymmetric bridge, the *meso*-ΛΔ compound is impossible.

In detail, we present herein the synthesis and characterization of seven new neutral binuclear iridium(III) complexes (**BB1**, **BB2**, **BY1**, **BY2**, **YB1**, **YB2** and **YY**) carrying 2-(2,4-difluorophenyl)pyridine (**Hdfppy** – "B" moiety) or 2-phenylbenzothiazole (**Hpbtz** – "Y" moiety) as cyclometalating ligands and **pic-O**$^{2-}$ as ancillary one (Figure 1).

For completeness, the properties of the obtained complexes are also compared with those of previously reported mononuclear analogues **B** and **Y** (**Scheme 1**). For compound **YY** we only obtained one diastereomer, due to the steric hindrance of the cyclometalated ligands (see below for more information). Indeed, even in the well-known μ-dichloro-bridged dimers, accessed via Nonoyama's protocol,[44] where the Ir–Ir distances are < 4 Å (such as the archetype $[Ir(ppy)_2(\mu\text{-}Cl)]_2$ dimer), only the less sterically congested *rac*-(ΔΔ'/ΛΛ') diastereomers have been reported to date.[22,41]

Since diastereomers have different chemical and physical properties, we have separated and fully characterized all of them, which is something not always done when binuclear iridium(III) complexes are reported in literature (Table S1, Supporting Information). The electrochemical and photophysical properties have been investigated with the support of DFT calculations, and all the new compounds were tested as active materials in OLED devices.

2. Results and Discussion

2.1. Synthetic Procedures

The μ-dichloro-bridged dimers were formed reacting the cyclometalated ligand precursors (**Hdfppy** or **Hpbtz**) with $IrCl_3{\cdot}H_2O$ in a mixture of 2-ethoxyethanol and water. The mononuclear iridium complexes **B** and **Y** were obtained in the presence of Na_2CO_3 via the reaction of μ-dichloro-bridged dimers and the 3-hydroxypyridine-2-carboxylic acid (**Hpic-OH**) ancillary ligand. The strength of such base can only deprotonate the carboxylic group, and not the phenolic group. After SiO_2 column chromatography, pure **B** and **Y** were obtained in 77 and 84% yields, respectively (Scheme 1).

To obtain binuclear complexes, mononuclear compounds (**B** or **Y**) were reacted with 0.6 equivalents of the iridium(III) dimers ($[(pbtz)_2Ir(\mu\text{-}Cl)]_2$ or $[(dfppy)_2Ir(\mu\text{-}Cl)]_2$) in the presence of the stronger base NaOH in absolute ethanol (Scheme 1). This reaction leads to the formation of the homo binuclear complexes **BB** and **YY**, and the hetero binuclear **YB** and **BY**, in good yields.

Both diastereoisomers were obtained for all the complexes except **YY**, for which only the most stable one was obtained due to the higher steric hindrance of its cyclometalating ligands. To separate the diastereoisomers, the complexes were purified with a long and careful procedure that involves the use of celite and neutral alumina to remove unreacted reagents, and basified silica gel using diethyl ether as the sole eluent (see Supporting Information for further details).

2.2. Diastereoisomer Identification

After compound purification and in some cases recrystallization, detailed characterizations were carried out by ^{1}H, ^{19}F, ^{13}C and 2D NMR, and mass spectrometry (Figures S1–S9, Supporting Information).

As stated above, each complex (e.g., **BY**) comes as a couple of separable diastereoisomers (i.e., **BY1** and **BY2**); moreover, each diastereoisomer consists of a couple of enantiomers ΛΛ'/ΔΔ' (for **BY1**) or ΛΔ'/ΔΛ' (for **BY2**), where Λ (lambda) refers to a left-handed and Δ (delta) to a right-handed optically active iridium centre. Due to the asymmetric nature of our bridge, such chiral centres are never equivalent, so that the ΛΔ' and ΔΛ' enantiomers do not form *meso* compounds, even in the case of homonuclear complexes (i.e., **BB2**).

Despite several attempts, after the diastereoisomer separations, we could never obtain suitable crystals for X-ray diffraction

analysis to properly assign the proper stereochemistry of each sample. Consequently, the experimental ^{1}H-NMR spectra were compared to DFT simulated ones to properly identify the correct absolute configuration. To achieve this goal, all the protons of all compounds have been attributed through 2D NMR experiments (COSY, HSQC and HMBC), while Gauge-Independent Atomic Orbital (GIAO) method was used to estimate their chemical shift in both possible diastereoisomers (see Supplementary Information for further details).

For each sample, the experimentally determined chemical shift of the 16 protons on the four N-coordinating rings of the cyclometalating ligands were correlated with the DFT-computed ones for both diastereoisomers. Indeed, such 16 protons are expected to be more affected by the different isomer conformation since the N-coordinating rings interact differently through space within each other and the bridging ligand, depending on the diastereoisomer; on the contrary, the phenyl moieties have much more similar spatial arrangement within each diastereoisomer couple. In Figures S10–S13 (Supporting Information) are reported the correlation graphs, showing that the experimental ^{1}H chemical shifts of each sample correlate well with the calculated chemical shifts of just one diastereoisomer, as numerically demonstrated by 3-to-40 times lower chi-square values for the correct match. For example, in the case of **YY** (where only one diastereoisomer is experimentally obtained), the correlation with the ΛΛ'/ΔΔ' relative configuration has a χ^2 value of 0.047, while $\chi^2 = 1.004$ if correlated to the wrong ΛΔ'/ΔΛ' counterpart. Less remarkable differences are found for the **BB** couple since such complexes have shorter cyclometalating ligands, resulting in fewer through-space interactions between the 16 pyridine protons of the two iridium centres. From these tests, it results that **BB1**, **BY1**, **YB1** and **YY** complexes are the ΛΛ'/ΔΔ' diastereoisomers, while **BB2**, **BY2** and **YB2** are the ΛΔ'/ΔΛ' ones.

These results are further confirmed by NOE NMR experiments carried out on the **BY** couple (i.e., **BY1** and **BY2**). Having previously attributed the chemical shifts of all protons, it was easy to decide which signals to monitor in NOE experiments. For each diastereoisomer, when the closest proton to each of the four nitrogen atoms of the cyclometalating ligands was selectively irradiated (i.e., protons 1, 7, 13 and 21 of **BY** in Figure 1), completely different NOE effects were obtained for **BY1** and **BY2** (Figures S14–S21, Supporting Information). Only at distances below 4 Å, the NOE effect is observed on spatially close protons. Accordingly, we could confirm that **BY1** is indeed the ΛΛ'/ΔΔ' diastereoisomer, while **BY2** is ΛΔ'/ΔΛ' (see Supplementary Information for further details).

2.3. Theoretical Calculation: Ground-State Properties

DFT calculations were used to optimize the ground-state geometry of all the binuclear complexes, considering both couples of diastereoisomers for each compound. The mononuclear complexes **B** and **Y** were also included in the investigation for comparison.

Calculations reveal that the difference in free energy between each couple of diastereoisomers is minimal for **BB1** and **BB2** (ΔG < 0.02 eV), since they are equipped with the smaller cyclometalating ligands. A similar scenario is observed for the structural isomer couples **BY** and **YB**: the four compounds are close in energy, with **BY2** and **YB2** that are the most stable isomers, and **YB1** and **BY1** that are just 0.02 and 0.03 eV higher in energy. On the contrary, DFT calculations nicely justify why the ΛΛ' and ΔΔ' stereoisomer are the only ones observed in **YY**, since the ΛΔ' and ΔΛ' counterparts are computed to be less stable by 0.10 eV, resulting in a Boltzmann ratio of 98:2 at 298 K.

In **Figure 2** are reported the frontier molecular orbitals (FMOs) of all the seven investigated binuclear complexes. Despite the complexity of the overall picture, some evident patterns are found: 1) All HOMOs and HOMOs–1 are centred on the phenyl moieties of the cyclometalating ligands and on the *d* orbitals of the nearby iridium(III) ion, as commonly observed in literature for similar mononuclear complexes;[2,45] HOMOs–2 are predominantly located on the 3-oxidopicolinate bridge with some contribution from the iridium centre chelated in the OˆO mode. 2) Despite the short bridging ligand, the energy and the topology of all the FMOs, which are mainly localized on individual ligands, are minimally perturbed by the presence of whatever kind of complex on the other side of the bridge; consequently, the lowest π^* orbital centred on the picolinate ligand is always located at ≈−1.55 eV in all binuclear complexes and the main factor determining the energy of a FMO centred on specific cyclometalating ligands is just the asymmetric nature of the bridge, which can coordinate each iridium centre using the NˆO or OˆO chelation mode. 3) Occupied and unoccupied FMOs centred on analogous cyclometalating ligands are stabilized by 0.17 or 0.06 eV, respectively, when located on ligands coordinating a NˆO-chelated iridium(III) ion. 4) No remarkable differences are observed within each pair of diastereoisomers.

The highest occupied orbital of the series is the one centred on the phenylbenzothiazole (pbtz) ligands coordinated to an OˆO-chelated iridium(III) ion (as in **YY** or **BY** complexes), which is located at ≈−5.52 eV. The highest occupied orbital centred on the difluorophenylpyridine (dfppy) ligands coordinated to an OˆO-chelated iridium(III) ion (as in **YB** or **BB** complexes) is more stable and found at ≈−5.68 eV, just ≈0.02 eV above the analogue centred on the pbtz ligands of a NˆO-coordinated complex (as in **YY** or **YB**). On the other hand, the highest occupied orbital on the dfppy ligands chelating a NˆO-coordinated iridium ion is the most stabilized one and it is found at −5.86 eV (as in **BY** or **BB** complexes).

The lowest unoccupied orbitals of all the series are the pairs centred on the pbtz ligands of NˆO-coordinated complexes (as found in **YY** or **YB**), closely followed by their analogues on the OˆO-bridged units (as in **YY** and **BY**). At higher energy are found the lowest pairs of π^* orbitals centred on the dfppy ligands, which are strongly mixed with the π^* orbitals of the picolinate bridge, due to their comparable energy; once again, such π^* orbitals are lower in energy if located on dfppy ligands bonded to an NˆO-chelated iridium(III) ion.

2.4. Electrochemistry

The electronic properties of all the series were also experimentally explored by both cyclic and square-wave voltammetry, carried out in acetonitrile solution at 298 K (see Experimental Section for further details). Electrochemical data obtained by cyclic

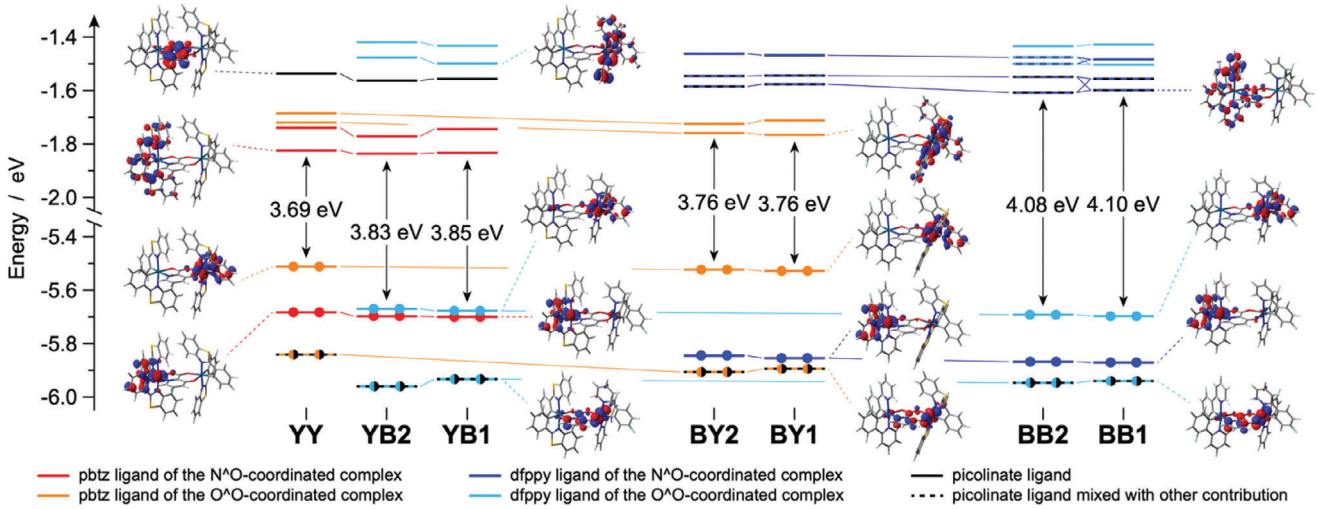

Figure 2. Energy diagram reporting the frontier Kohn–Sham molecular orbitals of all binuclear complexes in acetonitrile. Orbitals with similar topology are plotted with the same color for an easier comparison. For some relevant orbitals, the corresponding isosurface is also displayed (isovalue = 0.04 $e^{1/2}$ $bohr^{-3/2}$).

voltammetry for all the binuclear complexes and their reference compounds **B** and **Y** are summarized in **Table 1**, while the results of square-wave voltammograms are gathered and compared in Table S2 (Supporting Information). Due to poor solubility in acetonitrile, complex **YB1** was characterized in dichloromethane and compared to its **YB2** analogue in the same solvent (Table S3 and Figure S22, Supporting Information). All the observed redox processes are reversible.

To keep the discussion concise, the cyclic voltammograms reported in **Figure 3** (left) just refer to the ΛΛ' and ΔΔ' stereoisomers, since the ΛΔ' and ΔΛ' analogues essentially display the same redox properties, as demonstrated by Figure 3 (right) showing all the anodic side of the square-wave voltammograms of the whole series, including reference complexes **B** and **Y**.

The experimentally determined first and second oxidation potentials nicely confirm the DFT predictions about both the energy and the topology of the HOMO and HOMO–1 of all the binuclear complexes. The lowest oxidation process is observed at +0.504 V for **YY**, immediately followed by the first oxidation of **BY1** and **BY2** (i.e., +0.526 and +0.536 V, respectively); such processes can be easily attributed to the oxidation of the [$(pbtz)_2$Ir] moiety chelated by the bridging ligand in the O^O mode (compare Figures 2 and 3 right). At increasing potentials, the first oxidation process of **BB** and **YB** complexes is observed at +(0.686 ± 0.002) V, which is due to the oxidation of the O^O-chelated [$(dfppy)_2$Ir] moiety that all these complexes have in common; such a finding is again in line with DFT predictions (Figure 2). If potentials are further increased by just ≈0.13 V, the oxidation of the N^O-chelated [$(pbtz)_2$Ir] moiety is observed; indeed, such a process is only recorded for **YY** and **YB** complexes, as well as for the reference compound **Y** (Table 1). The highest oxidation process of the whole series is measured at +(1.00 ± 0.02) V and it is found as the second oxidation peak only in **BB** and **BY** complexes, since ascribable to the removal of one electron from the [$(dfppy)_2$Ir] moiety chelated by the bridging picolinate using its N^O side; accordingly, a similar oxidation potential is also found in the reference complex **B** (i.e., +0.954 V, Table 1).

Table 1. Electrochemical data of all complexes in acetonitrile solution (0.5 mM) + 0.1 M $TBAPF_6$ at 298 K.

	E_{ox} (ΔE_p)[a] [V (mV)]	E_{red} (ΔE_p)[a] [V (mV)]	ΔE_{redox} [b] [V]
BB1	+ 0.688 (62), + 1.014 (76)	−2.250 (69), −2.535 (150)	2.938
BB2	+ 0.688 (68), + 1.018 (72)	−2.253 (67), −2.535 (135)	2.941
BY1	+ 0.526 (65), + 0.985 (98)	−2.237 (74), −2.430 (187)	2.763
BY2	+ 0.536 (65), + 0.991 (81)	−2.230 (73), −2.458 (179)	2.766
YB1	[c]	[c]	[c]
YB2	+ 0.684 (66), + 0.836 (66)	−2.168 (67), −2.420 (76)	2.852
YY	+ 0.504 (60), + 0.806 (67)	−2.222 (73), −2.316 (66)	2.726
B	+ 0.954 (71)	−2.116 (73)	3.070
Y	+ 0.784 (67)	−2.132 (77)	2.916

[a] The reported potential values are obtained by cyclic voltammetry and reported *vs.* the ferrocene/ferrocenium couple, used as the internal reference. The value in parenthesis is the peak-to-peak separation from cyclic voltammetry (ΔEp); [b] $\Delta E_{redox} = E_{ox} - E_{red}$; [c] Not available due to poor solubility, check Supporting Information for data in dichloromethane.

Even the reduction processes are in line with the DFT predictions as the first reduction potential becomes more negative following the order: **YB** > **YY** > **BY** > **BB**; such experimental results are nicely correlated with the computed LUMO energies along the series (compare Table 1 and Figure 2). The attribution of these reduction processes can be easily assigned by looking at LUMOs topologies (Figure 2) and it is not further discussed. All second reductions can be ascribed to processes involving LUMO+1 and, within each complex, they have the same nature of the first reductions since LUMO and LUMO+1 come in pairs and are centred on analogue ligands (see previous section).

Finally, it is nice to point out that the electrochemical redox gaps nicely correlate with the HOMO–LUMO gaps calculated by DFT since they both increase in the order: **YY** ≈ **BY** < **YB** < **BB**. Notably, the redox gap between **BY** and **YB** increases by 0.09 V, in excellent agreement with the corresponding HOMO–LUMO gap increase of 0.08 eV; on the other hand, passing from **YB** to **BB**, a

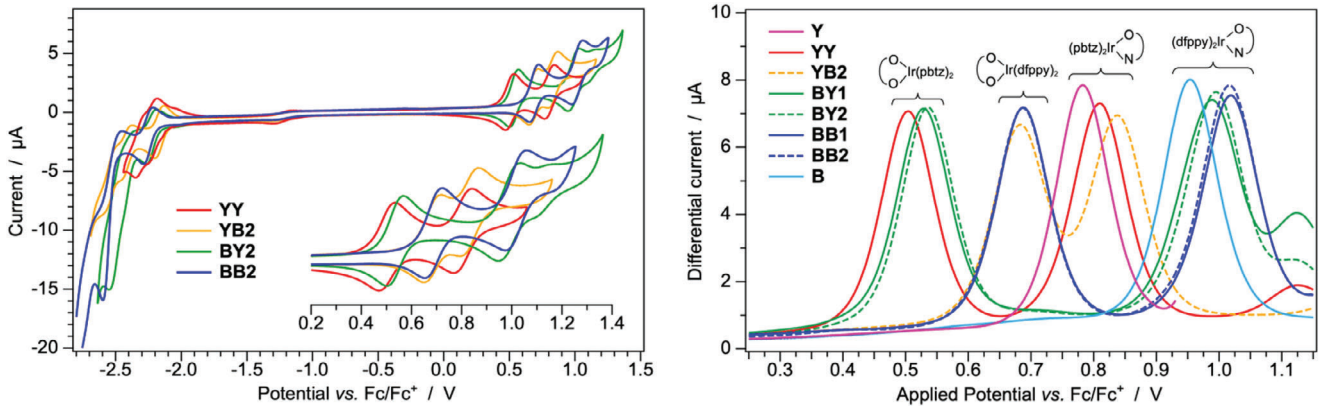

Figure 3. (Left) Cyclic voltammograms of selected stereoisomers of the binuclear complexes under investigation, with magnified anodic region. (Right) Anodic side of the square-wave voltammograms of all complexes, together with their reference compounds **B** and **Y**. All data were recorded in acetonitrile at 298 K.

redox-gap increase of 0.09 V is observed, while a larger increment of 0.25 eV is estimated by DFT calculations.

2.5. Photophysical Properties and Excited-State Calculations

The absorption spectra in room-temperature acetonitrile solution are reported in **Figure** 4a for all the binuclear complexes, together with the reference compounds **B** and **Y**.

As previously found by DFT calculations and electrochemical experiments, no noticeable differences are observed if comparing analogous stereoisomers (e.g., **YB1** and **YB2**) since they present both identical profiles and molar absorption coefficients (ϵ). It is also worth noting that the homo-binuclear complexes **BB** and **YY** have almost the same absorption features of the reference compounds **B** and **Y**, respectively, but their spectra display approximately twice the ϵ values of the mononuclear analogues, consistently with the presence of two iridium(III) centers.

The absorption spectra of the structural isomers **BY** and **YB** display virtually identical molar absorption coefficients and very similar profiles at $\lambda < 400$ nm, containing the features of both **B** and **Y** model compounds. Remarkably, the spectrum of **BY** extends more to the red, up to 550 nm (Figure 4a); indeed, this is in line with the narrower HOMO–LUMO gap of **BY**, if compared to **YB** (Figure 2). As already suggested by both DFT and electrochemical data, the energy of the lowest electronic transitions increases in the order: **YY** ≈ **BY** < **YB** < **BB** (Figure 4a, inset). TD-DFT calculations were used to explore the triplet excited-state scenario of all the investigated complexes; a compact representation of such lowest triplet vertical excitations is reported in Figure 4b for all the binuclear complexes and a more detailed description of each transition is reported in Tables S4–S12 (Supporting Information), including reference compounds **B** and **Y**.

Once again, the energy of the lowest triplet states (T_1) of each binuclear complex increases in the order: **YY** ≈ **BY** < **YB** < **BB** (Figure 4b). Indeed, the lowest couple of triplet states of the whole series is centred on the 2-phenylbenzothiazole (pbtz) cyclometalating ligands chelating the iridium(III) ion linked to the bridge on its OˆO side; such states are located at (2.43 ± 0.02) eV above the ground state and are obviously present only in **YY** and **BY** complexes. At (2.49 ± 0.02) eV above S_0, the lowest triplets located on the pbtz ligands of the NˆO-chelated [$(pbtz)_2$Ir] moiety are found; such states are T_1 and T_2 in **YB** complexes, while correspond to T_3 and T_4 in **YY**. In all the complexes, the ^{3}LC π–π^* state centred on the bridging picolinate ligand is located at (2.58 ± 0.02) eV; notably, such a state is the lowest triplet (T_1) for **BB1** and **BB2** complexes, so that it is expected to be responsible for the emission of these complexes. The triplets centred on the dfppy cyclometalating ligands are much higher in energy (i.e., at ≈2.79 and 2.84 eV, if localized on the OˆO- or NˆO-chelated moieties, respectively) and are likely not involved in the emission of any of the investigated binuclear complexes.

The emission spectra of all the compounds are reported in Figure 4c, while all the related photophysical parameters are summarized in **Table** 2. As for the absorption, no important differences are observed in the emission properties within each couple of diastereoisomers. It should be mentioned that, in the case of the hetero-binuclear complexes **BY** and **YB**, it was not possible to selectively excite only the [$(dfppy)_2$Ir] or the [$(pbtz)_2$Ir] moiety due to the very similar absorption profiles of reference compounds **B** and **Y**. Anyway, emission spectra were always independent of the excitation wavelength proving a quantitative energy transfer between the two iridium moieties.

As estimated by TD-DFT, **YY** and **BY** complexes display the most red-shifted emission spectra with virtually identical excited-state properties: same emission profiles, photoluminescence quantum yields (PLQYs) of 55% and excited state lifetimes (τ) of 1.5 μs (Figure 4c and Table 2); this is compatible with a ^{3}LC state centred on the π-extended pbtz ligands attached to the OˆO-chelated [$(pbtz)_2$Ir] moiety, which is the one that **YY** and **BY** share. The emission spectra of the binuclear complexes **YB1** and **YB2** are blue shifted by ≈30 nm, if compared to **YY** and **BY**, since the emissive triplet is now centred on the cyclometalating ligands of the NˆO-chelated [$(pbtz)_2$Ir] moiety; this is in line with TD-DFT predictions and it is experimentally confirmed by the fact that the spectra of both **YB** complexes are comparable to the one of reference compound **Y**, with substantially similar emission properties (i.e., PLQYs ≈67% and $\tau \approx 2.3$ μs, Table 2). On the contrary, the emission spectra of **BB1** and **BB2** are very different to the one of their mononuclear analogue **B**; indeed, a much lower PLQY is

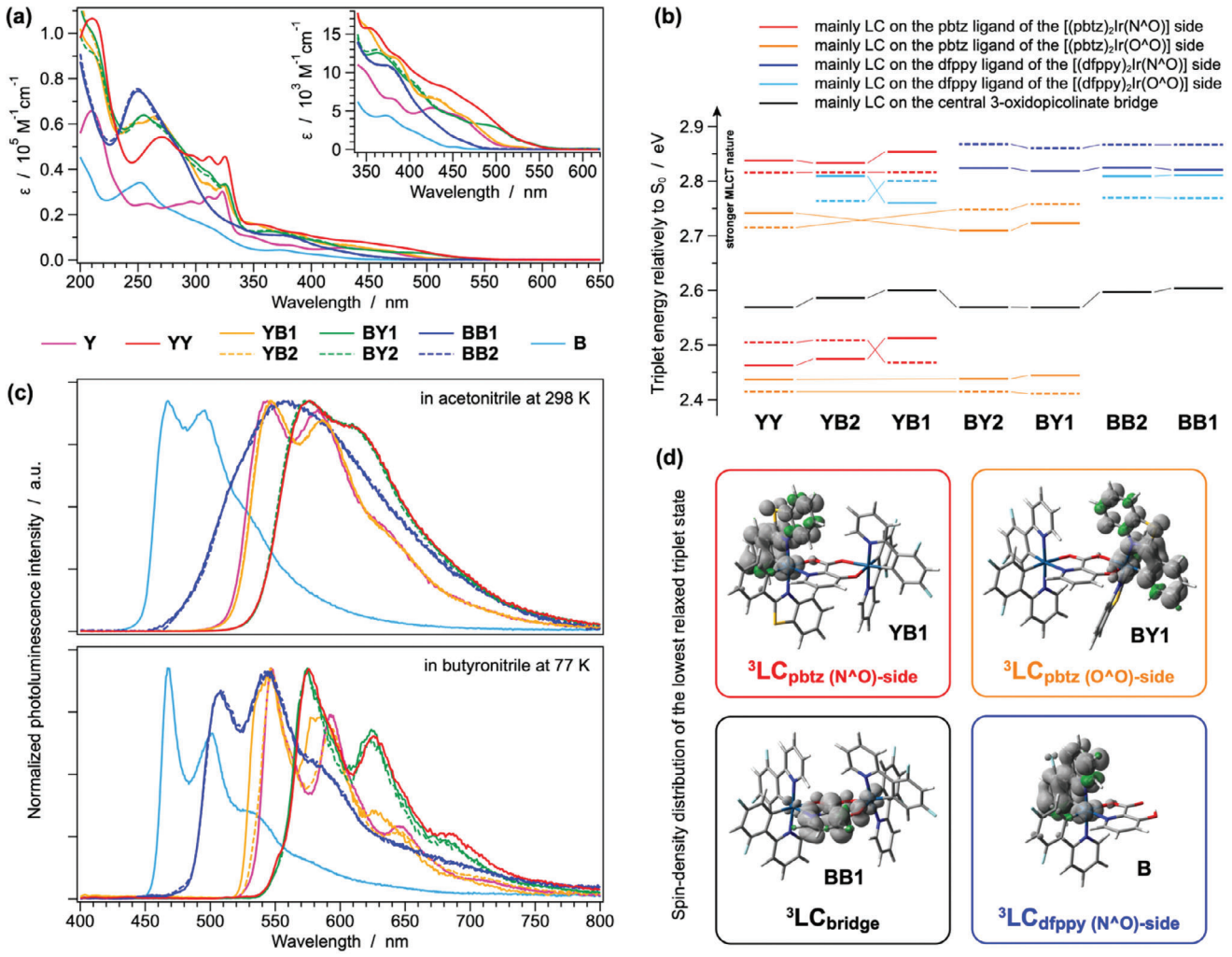

Figure 4. a) Absorption spectra in acetonitrile at 298 K and c) normalized emission spectra in the same conditions and in frozen butyronitrile glass of all the binuclear complexes, together with their reference mononuclear compounds **B** and **Y**. b) Energy diagram of the lowest-lying triplet states of all the investigated binuclear complexes, computed in acetonitrile as vertical excitations from the ground-state minimum-energy geometry; triplet states originating from excitations involving cyclometalating ligands in trans to the carboxylate moiety of the picolinate bridge are dashed. d) Spin-density surfaces of the lowest triplet state of selected complexes in their fully relaxed geometries (isosurfaces: 0.002 e bohr^{-3}).

observed for these binuclear complexes (i.e., 2 vs 49%) and their emission spectrum is strongly red shifted, if compared to the one of **B**. All these experimental findings confirm the TD-DFT predictions suggesting that **BB** complexes emit from a ^{3}LC state centered on the 3-oxidopicolinate bridge and not from a triplet state centred on the dfppy cyclometalating ligands, as in **B** (compare Tables S4,S5, and S11, Supporting Information).

The ligand-centred (LC) nature of all the phosphorescence spectra in room-temperature acetonitrile solution is confirmed by emission measurements in frozen matrix at 77 K (Figure 4c). Indeed, all the spectra at low temperature display just more resolved vibronic progressions, while no shifts are observed if comparing spectra recorded at 77 and 298 K (except for **BB** complexes, vide infra). The only remarkable difference in the photophysical properties at low vs. room temperature is the huge elongation in the excited-state lifetime of **BB** complexes (i.e., 0.1 vs 2.0 µs, respectively), accompanied by a stronger emission intensity.

All the above-mentioned attributions are entirely corroborated by spin-unrestricted DFT calculations (U-DFT), which were used to explore the nature of the fully optimized lowest triplet of all the investigated compounds (Figure 4d for selected examples). For the sake of conciseness, it is just worth mentioning that the T_1 state of **BB** complexes experiences an important excited-state distortion of the [(dfppy)$_2$Ir] moieties with respect to the bridge plane, if compared to the ground state geometry (Figure S23, Supporting Information); indeed, such deformation can justify: (i) the poorly-resolved vibronic profile of both **BB** complexes at 298 K (Figure 4c), despite the LC nature of the emissive states; (ii) the weak emission in room-temperature solution and the enhanced luminescence in rigid matrix at 77 K. Moreover, U-DFT calculations nicely predict that the adiabatic energy difference between T_1 and S_0 minima is ≈2.45 eV for both **BB1** and **BB2** complexes, while a larger gap is calculated for the mononuclear counterpart **B** (i.e., 2.75 eV); such theoretical findings nicely

Table 2. Luminescence properties and photophysical parameters of all the investigated binuclear iridium(III) complexes and mononuclear reference compounds (**B** and **Y**).

	Oxygen-free acetonitrile solution, 298 K					Butyronitrile, 77K		1% PMMA matrix, 298 K				
	λ_{em}[a] [nm]	PLQY[a] [%]	T[b] [μs]	k_r[c] [10^5 s^{-1}]	k_{nr}[d] [10^5 s^{-1}]	λ_{em}[a] [nm]	τ[b] [μs]	λ_{em}[a] [nm]	PLQY[a] [%]	τ[b] [μs]	k_r[c] [10^5 s^{-1}]	k_{nr}[d] [10^5 s^{-1}]
BB1	558	2.0	0.088	2.3	111	507, 544, 585[sh]	1.96	518[sh], 545	24.8	2.31[e]	–	–
BB2	558	2.1	0.098	2.1	100	508, 544, 585[sh]	1.95	518[sh], 545	26.9	2.50[e]	–	–
BY1	575, 608[sh]	54.9	1.49	3.69	3.03	575, 625, 680[sh]	4.71	571, 607, 660[sh]	54.4	1.45	3.75	3.14
BY2	575, 608[sh]	55.6	1.46	3.81	3.04	575, 624, 680[sh]	4.64	571, 609, 665[sh]	58.8	1.37	4.29	3.01
YB1	547, 586	66.2	2.24	2.96	1.51	547, 584, 628	2.67	547, 585, 628[sh]	65.8	2.07	3.18	1.65
YB2	547, 586	67.0	2.26	2.97	1.46	547, 593, 647	2.62	553, 585, 628[sh]	58.6	2.08	2.82	1.99
YY	576, 610[sh]	54.5	1.56	3.49	2.92	576, 626, 685	4.55	580, 607, 660[sh]	54.0	1.62	3.33	2.84
B	468, 495	49.2	2.40	2.05	2.12	468, 500, 530[sh]	2.45	465, 494	77.9	3.19	2.44	0.69
Y	544, 583	69.0	2.38	2.90	1.30	547, 593, 645	2.85	540, 580, 625[sh]	75.3	2.07	3.64	1.19

[a] λ_{exc} = 360 nm; [b] λ_{exc} = 373 nm; [c] Radiative constant: k_r = PLQY/ τ; [d] Non-radiative constant: k_{nr} = 1/ τ – k_r; [e] Major contribution (relative weight: 73–77%) of a biexponential lifetime, the minor component is ≈0.7 μs; [sh] Shoulder.

estimate the onset of the emission spectra of **BB** and **B**, respectively (Figure 4c).

The emission properties of the complexes were also investigated in the solid state as doped films of poly(methyl methacrylate) (PMMA) matrix at a concentration of 1% by weight (Figure S24, Supporting Information and Table 2). Both emission spectra, photoluminescence quantum yields, and excited-state lifetimes resemble the one recorded in solution at 298 K, if not for a slightly more pronounced vibronic progression in the emission bands. The only notable exception is a tenfold increase in the PLQYs of **BB** complexes, which is again compatible with restricted excited-state distortions due to the rigid polymeric matrix that can limit non-radiative deactivation pathways, as already observed in the frozen matrix at 77 K (Table 2).

2.6. Electroluminescence Properties

To explore a potential application of such novel class of binuclear complexes, we evaluated their electroluminescence (EL) properties in solution-processed organic light-emitting diodes (OLEDs), along with the ones of the two mononuclear reference compounds **B** and **Y**. According to the high PLQYs shown both in solution and at the solid state (Table 2), such iridium(III) complexes were used as guests in a host:guest emissive layer (EML).

For the development of OLEDs, the following device architecture was adopted: glass/Indium Tin Oxide (ITO)/ poly(3,4-ethylenedioxythiophene) polystyrene sulfonate (PEDOT:PSS)/ poly(9-vinylcarbazole) (PVK): 1,3-bis[2-(4-tert-butylphenyl)-1,3,4-oxadiazo-5-yl]benzene (OXD-7): 3.3 wt % iridium(III) complex/LiF/Al (**Figure 5a**). Although the device structure could be optimized in terms of operation and performance, a simple and solution-processable benchmark architecture was selected in this work for the sake of comparing the electroluminescence characteristics of the reported binuclear complexes.[46] In the device, PEDOT:PSS was used to favour the injection of holes into the EML,[47] while LiF acted as the electron injection layer. In addition to that, it is worth mentioning that the presence of OXD-7 in the EML was necessary to guarantee a suitable device operation. Indeed, OXD-7 is known to provide a good balance of opposite charge carriers in the EML, due to its great electron-transport ability, when combined with PVK.[48] Figure 5b shows the EL spectra of all OLEDs including the binuclear complexes or their mononuclear reference compounds, while a detailed analysis of their characteristics is reported in **Table 3**. In all cases, the two diastereomers of the same complex led to devices with similar

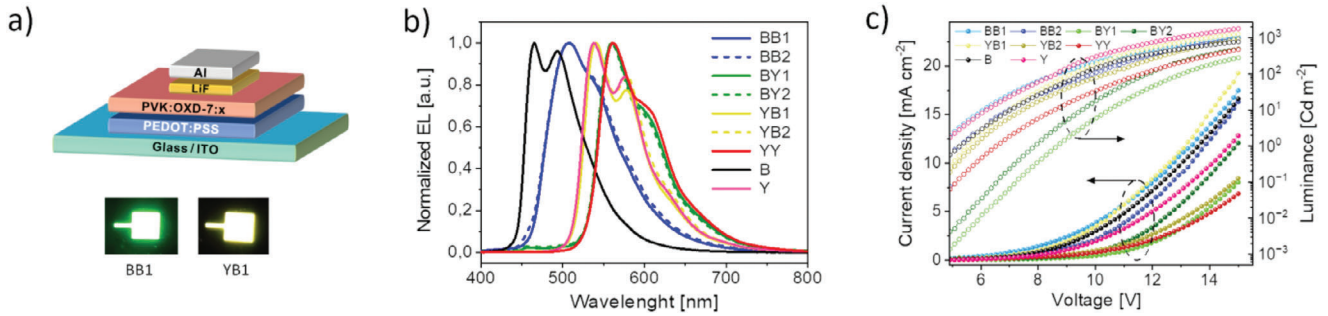

Figure 5. a) Schematics of the OLED structure including each of the investigated iridium(III) complexes as guest (x) in the emissive layer (top panel) and pictures of devices (bottom panel), in the ON state, including **BB1** and **YB1**; b) Normalized electroluminescence spectra of all the fabricated OLEDs; current density (filled dots) and corresponding luminance (empty dots) of all OLEDs as a function of the applied voltage.

Table 3. Optoelectronic characteristics of OLEDs.

	λ_{EL} [nm]	Color coordinates [x,y]	V_{ON} [a)] [V]	EQE [b)] [%]	Luminance [b)] [cd m^{-2}]	CE [b)] [cd A^{-1}]	PE [b)] [lm W^{-1}]
BB1	507, 535 [sh)]	0.32, 0.56	4.5	2.2	1016	6.5	1.4
BB2	507, 536 [sh)]	0.33, 0.56	5.3	2.4	944	6.4	1.3
BY1	561, 599 [sh)]	0.51, 0.47	8.7	1.8	281	5.4	1.1
BY2	561, 598 [sh)]	0.51, 0.47	7.9	1.6	490	5.1	1.1
YB1	539, 577	0.46, 0.53	5.6	2.6	1283	11.7	2.5
YB2	538, 577	0.46, 0.53	5.8	2.5	927	11.5	2.4
YY	561, 602 [sh)]	0.53, 0.47	6.6	2.9	477	8.2	1.7
B	465, 493	0.20, 0.41	8.2	3.2	782	5.5	1.2
Y	538, 577	0.47, 0.52	8.9	6.6	1804	16.4	3.4

[a)] At a luminance of 1 cd m^{-2}; [b)] At a driving voltage of 15 V; [sh)] Shoulder

EL spectra. Specifically, OLEDs based on **BB1** and **BB2** showed light emission with a peak wavelength of 507 nm and a shoulder at ≈535 nm; therefore, a green emission was recorded and the Commission Internationale de L'Eclairage (CIE) coordinates resulted to be ≈(0.32, 0.56). A progressive red-shift of the EL peaks was observed for **YB**, **BY** and **YY** complexes; accordingly, a gradual variation of the CIE coordinates of related OLEDs is also observed, and emission color changes from green to yellow and orange (Figure S25, Supporting Information). This trend correlates well with photoluminescence (PL) spectra in doped PMMA matrix (Figure S24, Supporting Information). Nevertheless, for the binuclear emitters, a slight blue-shift is observed when comparing EL spectra of OLEDs and PL spectra of PMMA films (≈10 nm for **BB**, **YB** and **BY**; ≈20 nm for **YY** complex). The spectral variation is most likely ascribed to the different dielectric environment of the host in EML with respect to the PMMA matrix, with the consequent possible rigidification of the emissive moieties in the environment of the host matrix.[49] This assumption is further confirmed by the emissive wavelengths and full width at half maximum of EL spectra that are similar to those of PL spectra measured at 77 K (Figures 4c and 5b).

Overall, the features of all EL spectra are clearly ascribed to the characteristics of the iridium(III) complexes, while possible contributions of the PVK-OXD-7 matrix are not visible. An efficient energy transfer is therefore obtained in all devices.

Furthermore, the optoelectronic characteristics of all the devices based on the binuclear emitters are in accordance with those of OLEDs having a similar architecture (Figure 5c and Table 3),[48] highlighting that all binuclear complexes are promising phosphorescent emitters for device applications. In addition, it should be emphasised that their OLED performances are basically comparable to the ones having the mononuclear **B** and **Y** emitters in the active layer. Specifically, the current density of all OLEDs shows a good diode-like behavior as a function of the applied voltage (Figure 5c). A slight variation of the maximum luminance is instead measured depending on the chemical structure and/or molecular weight of the emissive complexes.

Generally, OLEDs show different figures of merit depending on the emitter, while different diastereomers of the same complex provide similar characteristics to the device. For instance, OLEDs based on **YB1** and **YB2** complexes show external quantum efficiency (EQE) of 2.6% and 2.5%, luminance of 1283 and 927 cd m^{-2}, current efficiency (CE) of 11.7 and 11.5 cd A^{-1}, and power efficiency (PE) of 2.5 and 2.4 lm W^{-1} (Table 3). In comparison, OLEDs based on **BY** complexes exhibit lower performance as evidenced by EQE of ≈1.7% and PE of 1.1 lm W^{-1}. This decrease is compatible with the PLQY of the **BY** diastereomers, which is more than 10% lower than that of **YB** complexes (Tables 2 and Table 3).

Poor correlation with their relative PLQY is instead shown by **BB1**, **BB2**, and **YY** complexes. OLEDs based on **BB1** and **BB2** show a high EQE of 2.2% and 2.4% even though the PLQY in the PMMA matrix is ≈24.8% and 26.9%, respectively. The excited state of both **BB** diastereomers is however strongly influenced by the environment and, as evidenced by the blue shift of the EL spectra compared to the PL spectra in PMMA, the host matrix of the EML is likely restricting the distortion to further promote radiative deactivation pathways. Similar considerations can justify the relatively high performance of **YY**-based devices, which show the highest EQE of the series of 2.9%. However, **YY**-based devices are characterized by a relatively low luminance of 477 cd m^{-2}, which can be ascribed to a limited current density at the maximum applied voltage (Figure 5c). As a result, the efficient operation of the device is offset by constraints of electrical conductivity. Similar limitations are observed in **BY**-based OLEDs, as they show a relatively poor maximum luminance that can be ascribed to a suboptimal electrical operation of the device. The turn-on voltage is indeed the highest among all devices (Table 3). The analogous behavior between **BY** and **YY** compounds correlates well with the similarity of the energy (2.43 ± 0.02 eV) and localization of the lowest triplet state (T_1 is indeed centered on the 2-phenylbenzothiazole cyclometalating ligands chelating the iridium(III) ion linked to the bridge on its O^O side, Figure 4b). HOMO levels are also similar for both complexes as they are localized on the same position, and they have also the highest energy among all binuclear compounds (Figure 2 and Table 2). It is likely that the interaction of the phosphorescent emitters with the mixed host matrix (PVK and OXD-7) plays a major role on the electrical operation of the EML layer, that therefore has an influence on the device performance.

Overall, all binuclear complexes exhibit promising characteristics as phosphorescent emitters of solid-state devices. Among all, the combination of a high PLQY and the good electrical operation allows **YB** to produce OLEDs with the best PE (2.4 – 2.5 lm W^{-1}).

To note, although a roll-off of the EL efficiency typically occurs in OLEDs as the luminance increases, negligible variation of the EQE was observed even at the maximum luminance (Figure S26, Supporting Information), thus suggesting the absence of effects of annihilation or quenching which could be correlated to detrimental molecular aggregation.[48]

3. Conclusion

Seven binuclear cyclometalated iridium(III) complexes were effectively synthesized and structurally characterized by combined NMR and DFT techniques. The use of the simple and asymmetric 3-oxidopicolinate bis-anionic bridge (**picO**$^{2-}$) allows to obtain neutral both homo- (**BB** and **YY**) and hetero-cyclometalated (**BY** and **YB**) binuclear complexes with inequivalent iridium centres. Due to the small size of the bridging ligand, two couples of diastereoisomers (the racemic ΛΛ'/ΔΔ' pair and the ΛΔ'/ΔΛ' one) were isolated for all the compounds, except for the most sterically congested **YY** complex.

All the compounds were fully characterized by TD-DFT, electrochemical and photophysical methods allowing to unambiguously attribute the lowest-lying excited states. All the complexes display fully reversible reduction processes and emit from ^{3}LC excited states centred on the bridge (in the case of **BB** complexes) or ^{3}LC states located on the [(pbtz)$_2$Ir] moiety (the N^O-chelated for **YB** and the O^O-chelated one for **BY** and **YY**); such findings demonstrate a quantitative energy transfer between the two iridium units. Notably, the binuclear complexes display the same high PLQYs (up to 67%) of the related mononuclear analogues (**B** and **Y**), but with shorter lifetimes (so higher k_r). Accordingly, as a potential application for such a novel class of emitting molecules, we successfully tested them as active materials in OLEDs, reaching EQE, luminance, CE and PE of ≈2.5%, 1200 cd m^{-2}, 11.7 cd A^{-1}, and 2.5 lm W^{-1}, respectively, in a simple and solution-processed device architecture. Depending on the type of binuclear complex, green-to-orange emission was obtained with almost no efficiency roll-off over 1000 cd A^{-1}.

The present work paves the way for the easy and effective synthesis and characterization of binuclear metal complexes with short asymmetric bridges, which may be useful for exploiting two potentially emitting centres in one single molecule in light-emitting devices or in an antenna-emitter configuration. In addition, the present strategy can also be used to take advantage of quantitative energy-transfer processes to easily synthesize photosensitizer-(photo)catalyst pairs for applications in photocatalysis.

Supporting Information

Supporting Information is available from the Wiley Online Library or from the author.

Acknowledgements

This research was funded by the European Commission in the framework of H2020-MSCA-IF-2018, project ID 842633 "Lefko-Phos" and supported by PNRR Mission 04, Component 2, Investment 1.5 (project ECOSISTER – Ecosystem for Sustainable Transition in Emilia-Romagna, grant number ECS00000033, Concession Decree No. 1052 of 23/06/2022, within Spoke 1 – Materials for sustainability and ecological transition and Spoke 2 – Clean energy production, storage and saving). This work also received funding from the European Union's Horizon 2020 research and innovation programme under grant agreement no. 101016706 (h-ALO).

Open access publishing facilitated by Consiglio Nazionale delle Ricerche, as part of the Wiley - CRUI-CARE agreement.

Conflict of Interest

The authors declare no conflict of interest.

Author Contributions

K.S.B. and F.M. directed the project and funding acquisitions. K.S.B. and E.B. synthesized the compounds and performed the NMR characterization, supported by A.M. and A.B. The photophysical studies were carried out by K.S.B. and F.M.; F.M. was also responsible for the DFT and electrochemical characterizations. F.R., S.T., and M.P. prepared and tested the OLED devices. The original draft was prepared by K.S.B., A.B., M.P., and F.M.; all the authors reviewed and edited the final version.

Data Availability Statement

The data that support the findings of this study are available from the corresponding author upon reasonable request.

Keywords

asymmetric ligand, binuclear complexes, iridium(III) complexes, OLEDs

Received: June 14, 2024
Revised: August 8, 2024
Published online:

[1] S. Lamansky, P. Djurovich, D. Murphy, F. Abdel-Razzaq, H. E. Lee, C. Adachi, P. E. Burrows, S. R. Forrest, M. E. Thompson, *J. Am. Chem. Soc.* **2001**, *123*, 4304.
[2] F. Monti, A. Baschieri, L. Sambri, N. Armaroli, *Acc. Chem. Res.* **2021**, *54*, 1492.
[3] C.-H. Yang, M. Mauro, F. Polo, S. Watanabe, I. Muenster, R. Fröhlich, L. De Cola, *Chem. Mater.* **2012**, *24*, 3684.
[4] Y. Sun, X. Yang, Z. Feng, B. Liu, D. Zhong, J. Zhang, G. Zhou, Z. Wu, *ACS Appl. Mater. Interfaces* **2019**, *11*, 26152.
[5] L. He, L. Duan, J. Qiao, G. Dong, L. Wang, Y. Qiu, *Chem. Mater.* **2010**, *22*, 3535.
[6] M. Prosa, M. Bolognesi, L. Fornasari, G. Grasso, L. Lopez-Sanchez, F. Marabelli, S. Toffanin, *Nanomaterials* **2020**, *10*, 480.
[7] M. Bolognesi, M. Prosa, M. Toerker, L. L Sanchez, M. Wieczorek, C. Giacomelli, E. Benvenuti, P. Pellacani, A. Elferink, A. Morschhauser, L. Sola, F. Damin, M. Chiari, M. Whatton, E. Haenni, D. Kallweit, F. Marabelli, J. Peters, S. Toffanin, *Adv. Mater.* **2023**, *35*, 2208719.
[8] D. L. Ma, C. Wu, W. Tang, A. R. Gupta, F. W. Lee, G. Li, C. H. Leung, *J. Mater. Chem. B* **2018**, *6*, 537.
[9] A. Baschieri, S. Muzzioli, V. Fiorini, E. Matteucci, M. Massi, L. Sambri, S. Stagni, *Organometallics* **2014**, *33*, 6154.
[10] H. Yersin, in *Transition Metal And Rare Earth Compounds*, Springer, Berlin, Heidelberg **2004**, 1–26.

[11] M. Z. Shafikov, R. Daniels, V. N. Kozhevnikov, *J. Phys. Chem. Lett.* **2019**, *10*, 7015.
[12] N. C. Giebink, S. R. Forrest, *Phys. Rev. B* **2008**, *77*, 235215.
[13] P. T. Chou, Y. Chi, *Chem.-Eur. J.* **2007**, *13*, 380.
[14] X. Yang, X. Chen, J. Dang, Y. Sun, Z. Feng, Z. Tian, G. Zhou, Z. Wu, *Chem. Eng. J.* **2020**, *391*, 123505.
[15] A. Di Girolamo, F. Monti, A. Mazzanti, E. Matteucci, N. Armaroli, L. Sambri, A. Baschieri, *Inorg. Chem.* **2022**, *61*, 8509.
[16] A. Baschieri, L. Sambri, A. Mazzanti, A. Carlone, F. Monti, N. Armaroli, *Inorg. Chem.* **2020**, *59*, 16238.
[17] G. Zhou, C.-L. Ho, W.-Y. Wong, Q. Wang, D. Ma, L. Wang, Z. Lin, T. B. Marder, A. Beeby, *Adv. Funct. Mater.* **2008**, *18*, 499.
[18] B. Jiang, X. Ning, S. Gong, N. Jiang, C. Zhong, Z.-H. Lu, C. Yang, *J. Mater. Chem. C* **2017**, *5*, 10220.
[19] Y. Chi, T.-K. Chang, P. Ganesan, P. Rajakannu, *Coord. Chem. Rev.* **2017**, *346*, 91.
[20] G. Li, D. Zhu, X. Wang, Z. Su, M. R. Bryce, *Chem. Soc. Rev.* **2020**, *49*, 765.
[21] A. O. Adeloye, *Materials* **2019**, *12*, 2734.
[22] G. Li, D. G. Congrave, D. Zhu, Z. Su, M. R. Bryce, *Polyhedron* **2018**, *140*, 146.
[23] S. Bettington, M. Tavasli, M. R. Bryce, A. S. Batsanov, A. L. Thompson, H. A. Al Attar, F. B. Dias, A. P. Monkman, *J. Mater. Chem.* **2006**, *16*, 1046.
[24] A. Auffrant, A. Barbieri, F. Barigelletti, J. Lacour, P. Mobian, J. P. Collin, J. P. Sauvage, B. Ventura, *Inorg. Chem.* **2007**, *46*, 6911.
[25] X. Li, D. Zhang, W. Li, B. Chu, L. Han, T. Li, Z. Su, J. Zhu, Y. chen, Z. Hu, P. Lei, Z. Zhang, *Optical Materials* **2009**, *31*, 1173.
[26] J. L. Liao, P. Rajakannu, P. Gnanasekaran, S. R. Tsai, C. H. Lin, S. H. Liu, C. H. Chang, G. H. Lee, P. T. Chou, Z. N. Chen, Y. Chi, *Adv. Optical Mater.* **2018**, *6*, 1800083.
[27] W. Xiong, K. He, D. Zhang, J. Yang, M. Peng, Z. Niu, G. Li, W. Zhu, *J. Organomet. Chem.* **2022**, *959*, 122202.
[28] X. Yang, X. Xu, J. S. Dang, G. Zhou, C. L. Ho, W. Y. Wong, *Inorg. Chem.* **2016**, *55*, 1720.
[29] P. H. Lanoe, C. M. Tong, R. W. Harrington, M. R. Probert, W. Clegg, J. A. Williams, V. N. Kozhevnikov, *Chem. Commun.* **2014**, *50*, 6831.
[30] G. Li, X. Ren, G. Shan, W. Che, D. Zhu, L. Yan, Z. Su, M. R. Bryce, *Chem. Commun.* **2015**, *51*, 13036.
[31] H.-T. Mao, Y. Cui, G.-F. Li, G.-G. Shan, Q.-Y. Zeng, F.-S. Li, Z.-M. Su, *J. Mater. Chem. C* **2019**, *7*, 13461.
[32] A. M. Prokhorov, A. Santoro, J. A. Williams, D. W. Bruce, *Angew. Chem., Int. Ed.* **2012**, *51*, 95.
[33] X. Yang, Z. Feng, J. Zhao, J. S. Dang, B. Liu, K. Zhang, G. Zhou, *ACS Appl. Mater. Interfaces* **2016**, *8*, 33874.
[34] M. Z. Shafikov, A. V. Zaytsev, A. F. Suleymanova, F. Brandl, A. Kowalczyk, M. Gapinska, K. Kowalski, V. N. Kozhevnikov, R. Czerwieniec, *J. Phys. Chem. Lett.* **2020**, *11*, 5849.
[35] M. Z. Shafikov, R. Martinscroft, C. Hodgson, A. Hayer, A. Auch, V. N. Kozhevnikov, *Inorg. Chem.* **2021**, *60*, 1780.
[36] R. E. Daniels, S. Culham, M. Hunter, M. C. Durrant, M. R. Probert, W. Clegg, J. A. Williams, V. N. Kozhevnikov, *Dalton Trans.* **2016**, *45*, 6949.
[37] Y. Zheng, A. S. Batsanov, M. A. Fox, H. A. Al-Attar, K. Abdullah, V. Jankus, M. R. Bryce, A. P. Monkman, *Angew. Chem., Int. Ed.* **2014**, *53*, 11616.
[38] X. H. Yang, M. Li, H. Peng, Q. Zhang, S. X. Wu, W. Q. Xiao, X. L. Chen, Z. G. Niu, G. Y. Chen, G. N. Li, *Eur. J. Inorg. Chem.* **2019**, *2019*, 847.
[39] V. Chandrasekhar, T. Hajra, J. K. Bera, S. M. Rahaman, N. Satumtira, O. Elbjeirami, M. A. Omary, *Inorg. Chem.* **2012**, *51*, 1319.
[40] Q.-C. Zhang, H. Xiao, X. Zhang, L.-J. Xu, Z.-N. Chen, *Coord. Chem. Rev.* **2019**, *378*, 121.
[41] D. G. Congrave, Y.-t. Hsu, A. S. Batsanov, A. Beeby, M. R. Bryce, *Organometallics* **2017**, *36*, 981.
[42] G. Li, Y. Wu, G. Shan, W. Che, D. Zhu, B. Song, L. Yan, Z. Su, M. R. Bryce, *Chem. Commun.* **2014**, *50*, 6977.
[43] Y. Jiang, G. Li, W. Che, Y. Liu, B. Xu, G. Shan, D. Zhu, Z. Su, M. R. Bryce, *Chem. Commun.* **2017**, *53*, 3022.
[44] M. Nonoyama, *Bull. Chem. Soc. Jpn.* **1974**, *47*, 767.
[45] R. D. Costa, E. Orti, H. J. Bolink, F. Monti, G. Accorsi, N. Armaroli, *Angew. Chem., Int. Ed.* **2012**, *51*, 8178.
[46] W. Mróz, R. Ragni, F. Galeotti, E. Mesto, C. Botta, L. D. Cola, G. M. Farinola, U. Giovanella, *J. Mater. Chem. C* **2015**, *3*, 7506.
[47] M. Prosa, N. Li, N. Gasparini, M. Bolognesi, M. Seri, M. Muccini, C. J. Brabec, *Adv. Mater. Interfaces* **2017**, *4*, 1700776.
[48] F. Zhang, L. Duan, J. Qiao, G. Dong, L. Wang, Y. Qiu, *Org. Electron.* **2012**, *13*, 1277.
[49] S. Toffanin, R. Capelli, T. Y. Hwu, K. T. Wong, T. Plotzing, M. Forst, M. Muccini, *J. Phys. Chem. B* **2010**, *114*, 120.